Journal of Renewable Materials

Tech Science Press

DOI: 10.32604/jrm.2023.023400

ARTICLE

Elevated Temperature Properties of Bamboo Shaving Reinforced Geopolymer Composites

Xinli Zhang[1], Jiayu Zhang[1], Zuhua Zhang[2,*], Yiqiang Wu[1,*] and Yingfeng Zuo[1]

[1]College of Materials Science and Engineering, Central South University of Forestry and Technology, Changsha, 410004, China

[2]College of Civil Engineering, Hunan University, Changsha, 410082, China

[*]Corresponding Authors: Zuhua Zhang. Email: zuhuazhang@hnu.edu.cn; Yiqiang Wu. Email: wuyq0506@126.com

Received: 24 April 2022 Accepted: 15 June 2022

ABSTRACT

Geopolymer is a new alternative cement binder to produce concrete. In the present study, a novel geopolymer composites containing bamboo shaving (0–2 wt.%) were fabricated and exposed to the temperatures of 200°C, 400°C, 600°C and 800°C. Physical properties, micro-structure, and mechanical strengths of the geopolymer composites were evaluated before and after heating in order to understand their thermal properties, which are essential for the use as building materials. As the temperature rises, the drying shrinkage and apparent porosity of the composites increase, while the compressive and bending strengths decrease. At the temperature range of 200°C–800°C, the residual compressive strength rates of the geopolymer composite containning 2 wt.% bamboo shaving were respective 73.8%, 61.47%, 56.16%, and 29.56%, meanwhile, the residual flexural strength rates were respective 46.69%, 8.68%, 2.52%, and 2.33%. Correspondingly, the residual compressive strength rates of pure geopolymer were respective 72.81%, 61.99%, 54.55%, and 14.64%; the residual flexural strength rates were 48.87%, 5.69%, 3.22%, and 2.47%, respectively. Scanning electron microscope (SEM), optical microscope, and X-ray diffractometry (XRD) were applied to find the microscopic changes. The strength loss in the geopolymer composites was mainly because of the thermal degradation of bamboo shaving and shrinkage of geopolymer matrix. Bamboo shaving has great potential as reinforcer in developing low-cost geopolymer composites and may be used for applications up to 400°C.

KEYWORDS

Geopolymer composites; bamboo shaving; mechanical properties; high temperature; microstructure

1 Introduction

Ordinary Portland cement (OPC) is noncombustible and does not produce toxic gases or smoke when exposed to flames, which can provide sufficient fire resistance in most normal application [1,2]. However, sustained exposure to flame can cause severe spalling of OPC, resulting in structural damage and even collapse [3]. In addition, greenhouse gas emissions associated with OPC production have become a serious environmental problem.

In recent years, a novel eco-friendly and sustainable engineering material, known as geopolymer, has been rapidly developed as an alternative to OPC [4,5]. Geopolymer can be prepared by the reaction of aluminosilicate source materials and liquid alkaline activators. Apart from the environmental advantages,

geopolymer pastes and concretes also have the advantages of low shrinkage, low cost, high early-age strength, high chemical attack and fire resistance.

Several studies have been conducted on the synthesis, mechanics, and durability of geopolymer. Furthermore, fiber-reinforced geopolymer is increasingly being studied to achieve better mechanical properties [6–10]. The enhancement of basalt, polyvinyl alcohol (PVA), polypropylene (PP), cotton, and carbon fibers exhibited significant improved mechanical performance of geopolymer composites at room temperature [11–15]. But, when exposed in high temperatures, the strengths of the fiber-reinforced geopolymer composites obviously decreased because of fiber degradation or melting, as well as matrix shrinkage and cracking [16,17].

Welter et al. [18] examined the micro-structural evolution between fiber and matrix interactions in basalt fiber reinforced geopolymer composites after heating to 600°C–1000°C. They found the basalt fiber presented no significant degradation and that no micro-structural interaction existed within the matrix at 600°C. However, the crystallization and melting of basalt fibers increased with the increase in temperature, which made the brittle failure of the fiber and geopolymer composites increasingly obvious. After heating to 800°C and 1000°C, the softening of the basalt fiber could be observed, and several different diffusion processes between basalt fibers and the geopolymer matrix were evident. The interactions of fiber-matrix interactions after heating to 1000°C resulted in the formation of a crystalline albite phase. However, they did not study the mechanical properties of these composites after being exposed to high temperatures. Behera et al. [19,20] used almost the same test method to study the high-temperature properties of basalt microfibril and carbon microfiber reinforced geopolymer composites when exposed to 200°C, 400°C and 800°C, respectively. The results showed that the geopolymer composites with 10 wt.% basalt microfibrils content remained highest compressive strength at high temperature, and the respective strength loss was 32% at 400°C and 43% at 800°C. For the geopolymer composites containing 15 wt.% carbon microfibers, the residual compress strengths were 33.55 MPa and 23.96 MPa at 400°C and 800°C, and the minimum strength losses were 19% and 42%, respectively.

Tanyildizi et al. [21] studied the compressive and flexural strengths of geopolymer concrete with PVA fiber at 200°C–800°C. The results showed that curing conditions and fiber content had a certain influence on the strength values. For the samples with 2 wt.% fiber, the respective compressive strength reduction was 37% at 600°C and 49% at 800°C. At these two temperature values, the flexural strength exhibited a reduction like the compressive strength. The reductions were 11% and 44%, respectively. However, the compressive and flexural strengths at 400°C increased 29% and 45%, respectively. Celik et al. [22] compared the effects of four different fibers on the high-temperature behavior and mechanical performance of geopolymer composites. It was found that composites reinforced with PVA and basalt fiber exhibited a strength loss less than those of polyolefin and polyamide reinforced specimens at high temperatures. Within the range of 600°C–900°C, the compressive strength and flexural strength of synthetic fiber reinforced composites obviously decreased.

Alomayri et al. [23] investigated the effect of temperature (from 200°C to 1000°C) on the mechanical performance of fly-ash based geopolymer reinforced with cotton fabric. They found that the composites displayed decreased compressive and flexural strengths, and fracture toughness, along with the rise of temperature. Moreover, the mechanical properties were significantly reduced especially when the temperature was higher than 600°C. It was considered that the decrease of strength was due to the high-temperature degradation of cotton fiber and the increase of porosity in the composites.

Different from the results of the above studies, He et al. [24] reported a respective increase of 76% in flexural strength, 15% in work of fracture, and 75% Young's modulus of unidirectional carbon fiber reinforced geopolymer composites after 90 min at 1100°C. The property improvement could be attributable to the matrix densification and enhanced interface bonding strength. However, when heated to

1400°C, the mechanical properties lowered dramatically, which can be attributed to the serious degradation in carbon fibers, as well as the dissolving of the crystal phases and matrix melting.

To assess the suitability of geopolymer composites for high-temperature applications, Rickard et al. [25] conducted tests on geopolymer panels that were 50 mm thick under simulated fire conditions. They found that the fire resistance grading of above 60 min reached for all the test specimens of foamed and un-foamed geopolymer composites. It was considered that PP fiber could diminish pores collapses before gel solidification and alleviate high-temperature dehydration damage.

According to current research, different fibers have different effects on the properties of geopolymer composites. Unlike OPC, it was observed that the strength of geopolymer sometimes increases, and while at other times decreases, after exposure to high temperatures [26,27]. In a previous research, the authors of the present study reported a bamboo shaving (BS) reinforced geopolymer composite with good compressive and bending strengths [28]. The objective of this preliminary research was to study the change of compressive and flexural strengths, and micro-structure of geopolymer composites reinforced with BS at various temperatures (room temperature, and 200°C–800°C with an interval of 200°C), to provide some basic data for the subsequent in-depth study of the BS-reinforced geopolymer composites. Furthermore, thermo gravimetric analysis (TGA), scanning electron microscope (SEM), optical microscope, and X-ray diffractometry (XRD) were applied to investigate the thermal behavior and micro-structure of the BS reinforced geopolymer composites.

2 Experimental Methods

2.1 Materials

Metakaolin (MK, 1250 mesh fineness) was obtained from Inner Mongolia, China. It was a calcined product at 800°C for 3 h, used as the aluminosilicate source in the preparation of geopolymers. The chemical composition of MK was tested by X-ray fluorescence spectrometer and the result was given in Table 1. Bamboo shaving (BS) with the size of 3–5 mm was obtained from Yiyang Bamboo Industry Development Co., Ltd. (Hunan Province, China), and the main chemical constituents of the BS was around 41 wt.% cellulose, 28 wt.% lignin, and 10 wt.% hemicelluloses. The density and the moisture content of the BS are 0.68 g/cm^3 and 5.89%, respectively.

Table 1: Chemical composition of MK by mass (%)

Composition	SiO_2	Al_2O_3	Fe_2O_3	TiO_2	CaO	K_2O	MgO	P_2O_5	Na_2O	ZrO_2	Loss on ignition
Mass (wt.%)	50.13	42.55	3.41	2.40	0.45	0.35	0.17	0.15	0.15	0.11	0.13

The alkaline activator was combination of sodium silicate solutions (water glass) and solid sodium hydroxide (NaOH). The water glass was an industrial grade product containing 26.5 wt.% silica and 8.3 wt.% Na_2O (modulus Ms = 3.3). Analytically pure agent NaOH was obtained from Sinopharm Chemical Reagents Shanghai Co., Ltd., China.

2.2 Specimen Preparation

The alkaline activator was prepared from NaOH and sodium silicate, then cooled down to room temperature. MK (or mixed with BS) was added to the activator solution and stirred for 5 min. The obtained paste was rapidly poured into the moulds and vibrated for 3 min, then cured at room temperature for 24 h. The curing conditions of samples after demoulding were 60°C, and relative humidity (RH) ≥ 80% for 7 days.

The designed sample codes of the specimens are listed in Table 2. BS content is by the mass of MK.

Table 2: Mix proportion of BS reinforced geopolymer composites

Sample code	MK (g)	Alkaline activator (g)	BS content (wt.%)
GP	100	120	0
BSRGP1	100	120	1
BSRGP2	100	120	2

2.3 Exposure to High Temperatures

After curing, the specimens were heated to 200°C–800°C in turn using a muffle furnace to evaluate the strength change. The heating rate was 5 °C/min and maintained for 1 h after reaching the needed temperatures. The samples were taken out after natural cooling to room temperature in the furnace.

2.4 Characterizations

2.4.1 Thermo Gravimetric Analysis

Thermo gravimetric analysis (TGA) was carried out on the neat geopolymer (GP), BS, and BS reinforced geopolymer composites in flowing nigtrogen (20 ml/min) at a temperature rise rate of 10 °C/min. It was conducted using STA8000 therm-gravimetric analyzer (Perkin Elmer, USA) and the temperature range scanned from 30°C to 800°C.

2.4.2 Drying Shrinkage

The dimensions of samples before and after exposure to elevated temperatures were determined by a vernier caliper, the value of drying shrinkage (DS) was calculated using the Eq. (1):

$$DS = \frac{L_0 - L}{L_0} \times 100\% \tag{1}$$

where L_0 is the length of the samples at room temperature, and L is the length of samples after high temperature treatment.

2.4.3 Bulk Density and Apparent Porosity

The bulk density (D_b) and apparent porosity (P_a) were determined according to ASTM C20 and calculated using the Eqs. (2) and (3), respectively. Three specimens were tested and the results were the average of the three measured values.

$$D_b = \frac{m_d}{m_a - m_w} \tag{2}$$

$$P_a = \frac{m_a - m_d}{m_a - m_w} \times 100\% \tag{3}$$

In these two formulas, m_d is the weight of the dried specimen; m_a is the weight of the specimen saturated in air; m_w is the weight of the specimen suspended in water.

2.4.4 Water Absorption

Water absorption (WA) was determined referring to GB/T 5486–2008 and calculated using the Eq. (4). The size of samples was $40 \times 40 \times 40$ mm^3. Samples with an absolutely dry weight of m_0 were soaked in water at 20 ± 5°C for 24 h, then removed, wiped with a dry towel and weighted as m.

$$WA = \frac{m - m_0}{m_0} \times 100\% \tag{4}$$

2.4.5 Compressive and Flexural Strengths

The strength experiment was carried out according to the Chinese national standard GB/T 17671–1999. The size of test specimens for the compressive strength and flexural strength was 40 × 40 × 40 mm^3 and 40 × 40 × 160 mm^3, respectively. The tests were performed by using an electronic universal testing machine (MWD-50, Jinan, China) with a loading speed of 2.4 kN/s and 50 N/s for the compressive and flexural tests, respectively. Six and three specimens were respective measured for compressive and flexural tests, and the average calculated.

2.4.6 Microstructure Analysis

The changes in microstructure and morphological of geopolymer composites were studied by a SIGMA 300 field emission SEM (Zeiss, Germany) and an AO-FD600E optical microscope (Shenzhen Aoswei Optical Instrument Co., Ltd., China).

2.4.7 Phase Composition Investigation

The phase composition of the samples was studied by XRD. The analysis was conducted by an Empyren powder diffractometer (PANalytical, Netherlands) with Cu-Kα radiation (36 kV, 20 mA). A typical scan is from 10 to 80° with a scan speed of 0.02°/s.

3 Results and Discussions

3.1 Thermal Properties

The thermal stability of BS, GP, and BS reinforced geopolymer composites was investigated by TGA, with the analysis curves being shown in Fig. 1. Compared with GP and BS reinforced geopolymer composites, BS exhibits significant weight loss during this process and has three major stages (Fig. 1a). The first stage occurs between 30°C and around 200°C, where there is a small weight loss mainly induced by the evaporation of water in the BS, which is referred as to the moisture loss or drying stage. The second stage occurs from 200°C to about 365°C, the BS shows obvious weight loss, and the overall weight loss rate reaches 60%, which is mainly attributed to the rapid decomposition of cellulose and hemicelluloses due to the heating fracture, and it is accordingly called the rapid pyrolysis stage. As shown in Fig. 1b, the maximum weight loss rate was found at 339°C. This is because cellulose, hemicelluloses and lignin have different degrees of decomposition. However, due to their different pyrolysis peaks, the superposition effect causes the emergence of the main peak [29]. The third stage occurs from 365°C to 800°C, where BS carries on decomposition and retains 6% of its weight. It is the slow decomposition process of lignin and residue pyrolysis. Lignin is a complex aromatic polymer with wide bond energy distribution; its pyrolysis almost runs throughout the entire pyrolysis process [30]. The pyrolysis of lignin produces more fixed carbon, and therefore, the weight loss tends to be stable.

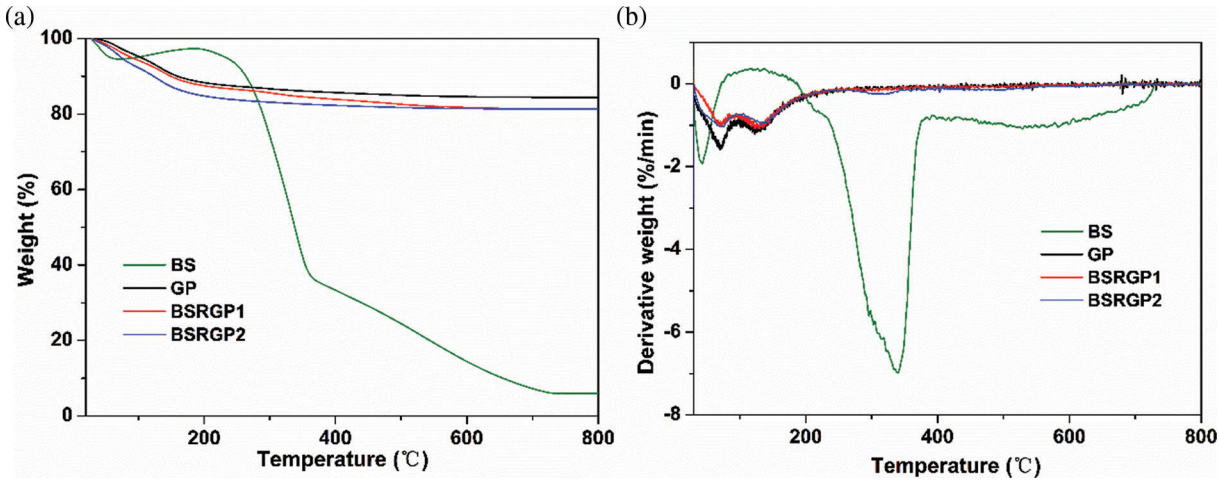

Figure 1: TGA (a) and DTG (b) curves of the BS, GP, BSRGP1, and BSRGP2

For the samples of GP, BSRGP1, and BSRGP2, all showed a dramatic drop of weight only below 200°C because of the evaporation of free moisture. Based on this behavior, it can be expected that the geopolymer will present very small shrinkage. When the temperature rises further from 200°C to 540°C, the three samples exhibit similar weight loss curves, probably due to the liberation of bound moisture and surface hydroxyl during the condensation reaction of the geopolymer, as well as the thermal decomposition of BS. This will further lead to surface micro-cracks and interior destruction to the whole architecture of the geopolymer. Their weight remains constant in the temperature range of 540°C–800°C, the residual weight of GP is 84.5% and that of BSRGP1 and BSRGP2 is 81.5%, indicating that the BS does not significantly deteriorate the thermal stability of the GP.

3.2 Physical Properties

The physical properties (such as drying shrinkage, porosity, density, and water absorption) of GP, BSRGP1, and BSRGP2 are investigated, with the results presented in Fig. 2. As shown in Figs. 2a and 2b, the shrinkage and apparent porosity of all samples increase with the increase in temperature. Furthermore, BSRGP2 has higher shrinkage and apparent porosity than both BSRGP1 and GP in the studied temperature range. This is consistent with the reported results of cotton fibers reinforced geopolymer composites at elevated temperatures [23]. In fact, the shrinkage and porosity of the composites are usually affected by many factors such as the amount and type of fiber fillers.

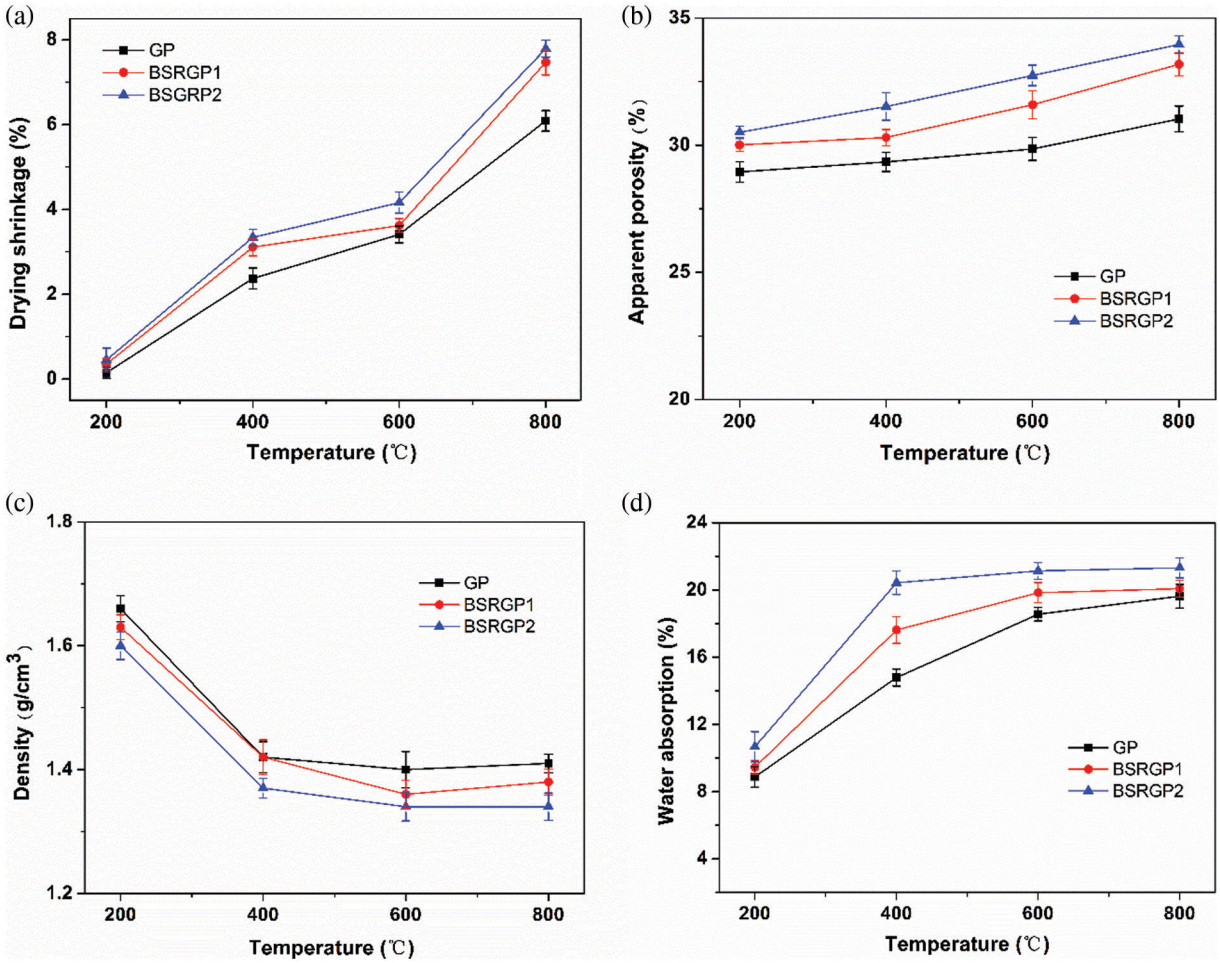

Figure 2: Drying shrinkage (a), apparent porosity (b), bulk density (c) and water absorption rate (d) of GP, BSRGP1, and BSRGP2 at high temperatures

The results of Fig. 2c show that the addition of BS decreases the density of the matrix. Meanwhile, the density of all samples decreases gradually with the increase in temperature, and it tends to be stable after 600°C, which is mainly due to the shrinkage of the geopolymer matrix and the degradation of the BS. Considering the test error, there is almost no difference between the data of 600°C and 800°C. In Fig. 2d, the water absorption increases across all three of the samples with increasing temperature and BS content, this has consistency with the porosity results in Fig. 2b. It may be attributable to the hydrophilicity of BS and the increase in porosity of the matrix due to the addition of BS.

3.3 Visual Inspection

Fig. 3 illustrates photographs of the visual inspection of GP, BSRGP1, and BSRGP2 at different temperatures. As can be seen from Figs. 3a–1 and 3a–5, no significant color change has occurred on the appearance of the GP, and there appears to be a slight lightening of color only at 200°C. With the rising temperature, macroscopic cracks gradually begin to appear. When exposed to 800°C, many cracks distribute on the outer surface and some spalling occurs; the sample is fragile. This is related to the destruction of the main-chains forming the geopolymeric system [22].

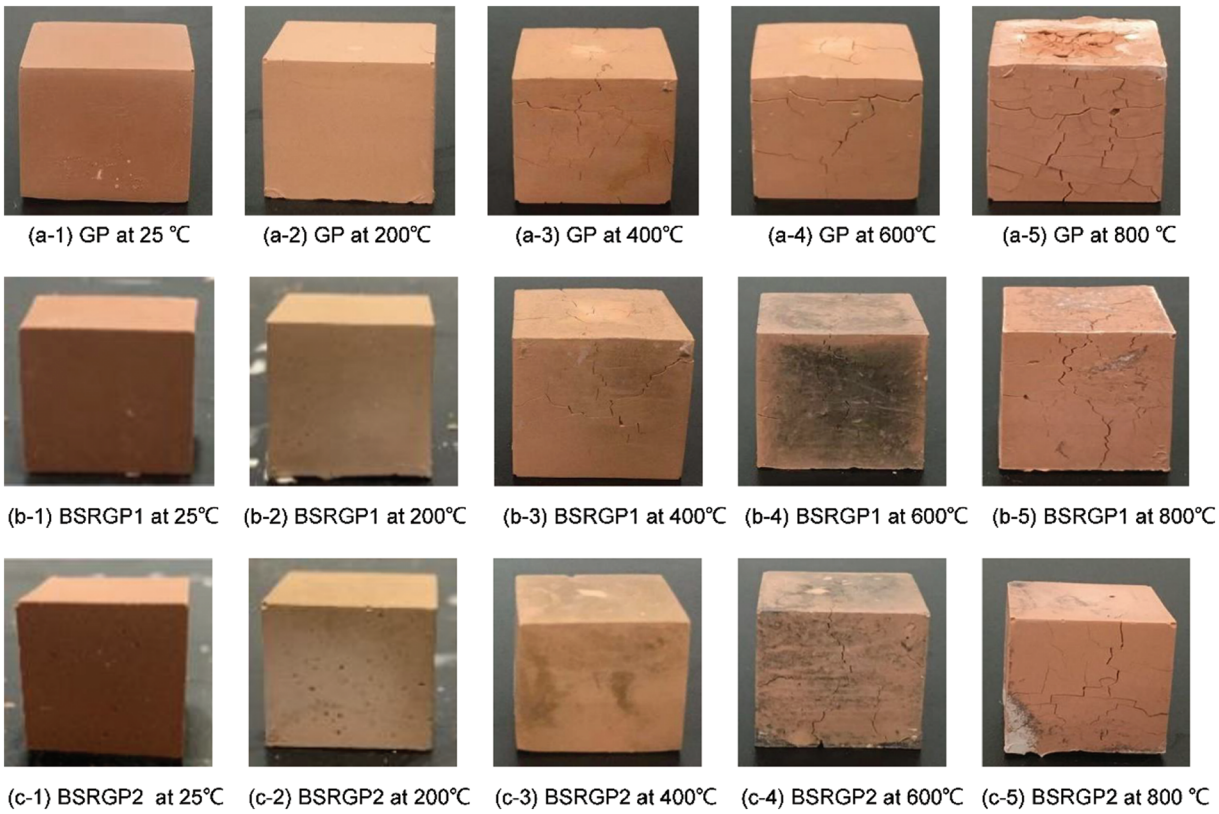

Figure 3: Visual inspection of GP, BSRGP1, and BSRGP2 at different temperatures

For the samples of BSRGP1and BSRGP2, both of their colors are the lightest at 200°C. Like GP, BSRGP1 begins to show networks of hairline cracks from 400°C. However, BSRGP2 does not show significant cracks until 600°C. At 600°C, both BSRGP1 and BSRGP2 have black carbides on their surfaces, but at 800°C, no black carbides are noticeable. Clearer cracks appear on the surfaces of the two samples at 800°C, and one corner of BSRGP2 is peeled off. The color change and cracks are useful as indicators of a significant loss in mechanical properties. This is because the appearance change is

consistent with an obvious decrease in strength caused by heating [31]. Compared with GP, BSRGP1 and BSRGP2 present fewer cracks. This indicates that BS plays a certain role in preventing high-temperature cracking due to the small voids formed by BS degradation inside the geopolymer matrix.

3.4 Mechanical Properties

The mechanical strength results of GP, BSRGP1 and BSRGP2 before and after heating are presented in Fig. 4. At room temperature, BSRGP1 and BSRGP2 have higher mechanical strength than GP. This is consistent with our previous research results [28], similar findings also can be found in cotton fiber reinforced geopolymer [32] and flex fiber reinforced geopolymer [33]. The compressive strengths of GP, BSRGP1, and BSRGP2 at room temperature are 50.27, 54.31, and 53.86 MPa, respectively. In the reference [28], the values of compressive strength of geopolymer with BS content of 0%, 1%, and 2% after 7 d curing were respective 43.44, 48.72, and 48 MPa. The mechanical strengths increase in this study may be due to the increase of curing temperature.

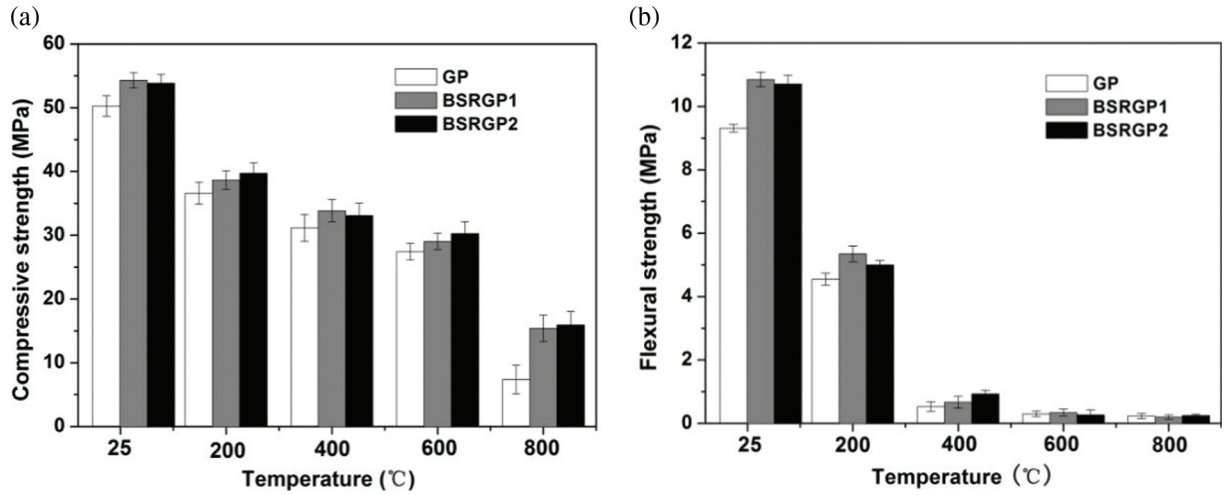

Figure 4: Compressive strength (a) and flexural strength (b) of GP, BSRGP1, and BSRGP2 at different temperatures

As shown in Fig. 4a, BSRGP1 and BSRGP2 possess a higher compressive strength than GP over all temperature ranges studied, while there are no significant differences in the compressive strengths between BSRGP1 and BSRGP2. The phenomenon can be explained from the good interfacial bonding between BS and geopolymer matrix, where BS limits the development of macroscopic cracks, which reduces the thermal stress of the geopolymer matrix at high-temperature exposure, thus maintaining a high residual compressive strength [34].

The compressive strength of all samples decreases with increasing temperature. After treatment at 800°C, the compressive strengths of GP, BSRGP1, and BSRGP2 were respectively 7.36, 15.39, and 15.92 MPa, and the residual strength rates were 14.64%, 28.34%, and 29.56%, respectively. The behavior may be attributable to the discharge of water moisture within the geopolymer to form voids and shrinkage cracks, as well as the thermal degradation of BS, leading to the loss of bearing capacity, which macroscopically shows as reduced compressive strength.

At present, there are few studies on the heat resistance of biomass geopolymer composites. Compared with the reference [23] on a study of cotton fiber reinforced geopolymer, the present research has an appropriate residual compressive strength of close to 30% at 800°C. However, the BS content is low in

this study. Of course, it is lower than that of basalt fiber reinforced geopolymer with the compressive strength residual rate higher than 39% at the same temperature [19].

Like that of the compressive strength, it can be observed from Fig. 4b that the flexural strength of the samples also decreases with increasing temperature, though the reduction is more serious, especially when the temperature is higher than 400°C. After the 400°C treatment, the flexural strengths of GP, BSRGP1, and BSRGP2 were respective 0.53, 0.67, and 0.93 MPa, and the residual strength rates were 5.69%, 6.18%, and 8.68%, respectively. After the 800°C treatment, the flexural strengths of GP, BSRGP1, and BSRGP2 were respective 0.23, 0.20, and 0.25 MPa, and the residual strength rates were 2.47%, 1.84%, and 2.33%, respectively. The main reason for the reduction in flexural strength may be due to the degradation, or combustion of BS, as well as the formation of small voids.

3.5 Micro-Structure Analysis

The SEM micro-graphs of GP, BSRGP1, and BSRGP2 at different temperatures are exhibited in Fig. 5. The micro-morphology of the aluminosilicate gel matrix with unreacted metakaolin plates and some tiny cracks distributed throughout was observed before high-temperature treatment (Figs. 5a–1). The BS is scattered in the matrix (Figs. 5b–1 and 5c–1), and the gap between the BS and geopolymer matrix is likely caused by the small shrinkage amount of aluminosilicate gel. The gap could offer a dehydration pathway for moisture upon exposure to elevated temperatures.

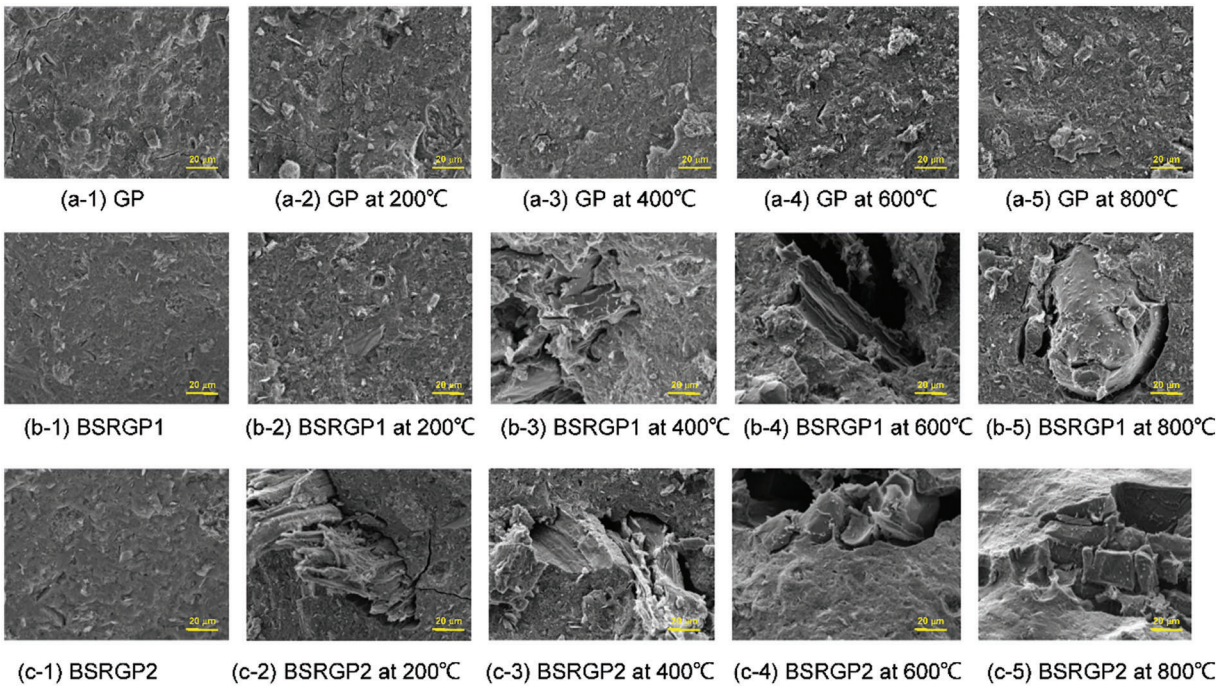

Figure 5: SEM images of the fracture surface for GP, BSRGP1, and BSRGP2 at different temperatures

When exposed to high temperatures, wide micro-cracks development and relatively large voids can be observed in the GP samples (Figs. 5a–2 and 5a–5). Beyond 400°C, the combustion and degradation of BS result in some irregular holes throughout the micro-structure of BSRGP1 and BSRGP2, as presented in Figs. 5b–3 and 5b–5 and 5c–3 and 5c–5, respectively. The porosity generated by BS degradation may reduce the internal vapor pressures, thereby reducing the possibility of cracking. These findings are also compatible with observations concerning the visual inspection in Fig. 3.

To investigate the changes of micro-structure in medium-length scales, optical microscope observation was performed, as the results presented in Fig. 6. Figs. 6(a–1) and 6(a–5) show the optical micro-graphs of GP exposed from room temperature to 800°C, whereby long cracks formed beyond 400°C which may be due to thermal shrinkage induced by dehydroxylation of the matrix of geopolymer.

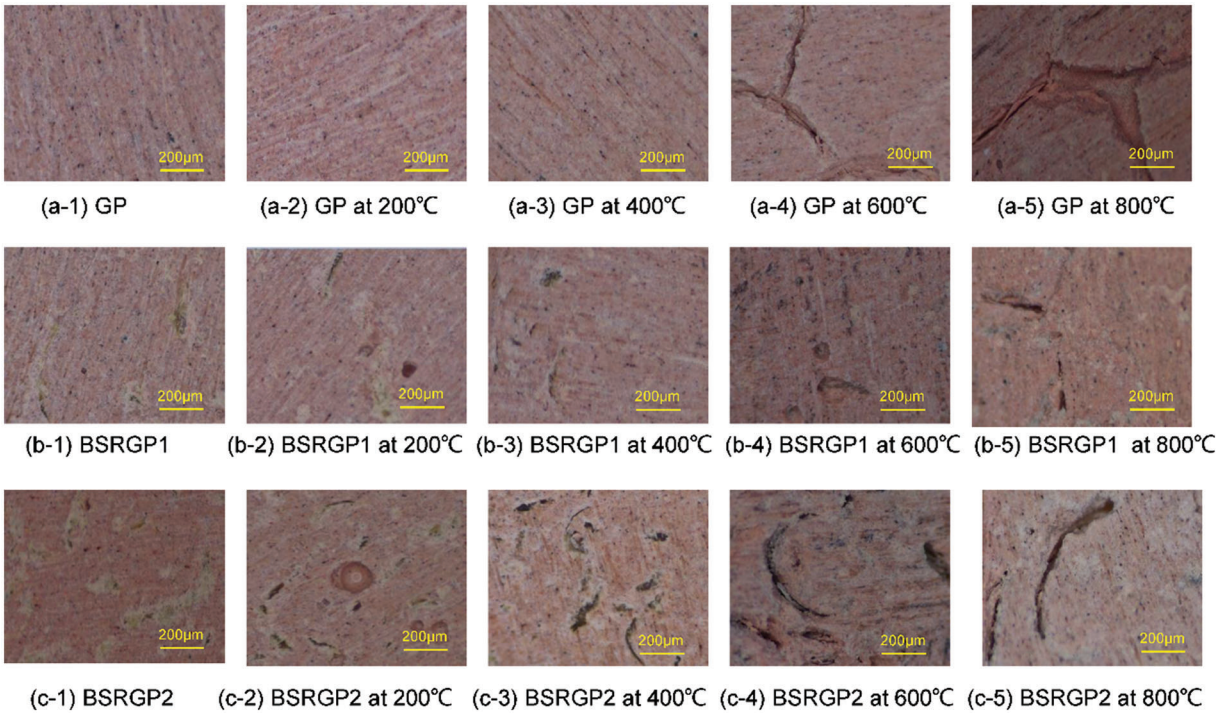

Figure 6: Optical micro-graphs of GP, BSRGP1, and BSRGP2 at different temperatures

In general, there is a certain adhesion degree between the matrix and fibrous fillers, and the presence of fibrous fillers has no chemical effect on the micro-structure of the prepared composites [22]. Figs. 6(b–1) and 6(c–1) represent the micrographs of BS reinforced geopolymer composites. The BS did not undergo any special pretreatment in this study. There is an acceptable interfacial adhesion between the BS and geopolymer, where such adhesion is related to the performance of the BS.

Figs. 6(b–2) and 6(c–2) show the optical micro-graphs of BSRGP1 and BSRGP2 at 200°C, the good state of the internal BS shows that the paste helps to prevent, or obviously reduce, the oxygen supply within the geopolymer composites. At 400°C (Figs. 6(b–3) and 6(c–3)), the BS is oxidized to a dark color but maintains its original form. However, there are no cracks in the matrix of composites like GP. As the temperature further increases, the BS is thermally oxidized into residue and leaves burned holes and voids in the matrix (Figs. 6(b–4), 6(b–5), 6(c–4) and 6(c–5)). Concerning the SEM micrographs of the samples after being exposed to 400°C–800°C (Fig. 5), the BS tends to degrade or melt above 400°C, which interprets the remarkable loss of strength after reaching this temperature (as presented in Fig. 4).

To further understand the distribution of BS in the geopolymer matrix and the formation of voids, the grayscale threshold method was selected for background segmentation, which can reserve the color information of BS and remove its background. The images in Fig. 6 were appropriately converted to binary form, and the results are shown in Fig. 7. For BSRGP1 and BSRGP2, the distribution of BS in the matrix is disordered and does not have a certain orientation Secondly, there are long cavities left in the

matrix caused by the high-temperature degradation of the BS, which act as water loss channels and reduce the possibility of forming large cracks in the matrix.

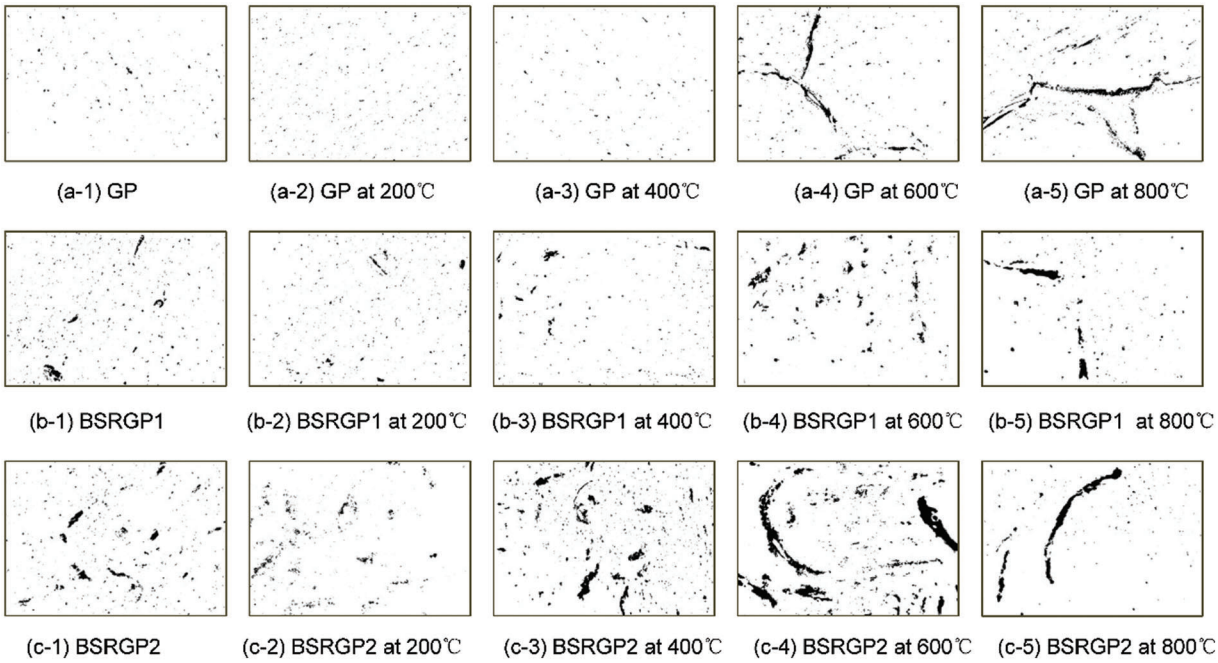

Figure 7: Understanding the distribution of the BS and voids in composites by image analysis

3.6 XRD Analysis

The phase composition of geopolymer composites was analyzed by XRD. The GP and BSRGP1 samples were selected as research objects. The XRD patterns before and after exposure to the temperatures of 200°C–800°C were exhibited in Fig. 8. For GP in Fig. 8a, the broad hump at 20–40° 2-theta is the typical feature peaks of geopolymer, indicating that the amorphous gels of geopolymerization are formed. The sharp diffraction peaks in this range come from the un-reactive silica and anatase in the raw material. It is easy to see that the peak patterns of GP samples are almost the same at room temperature and after the high temperature treatment of 200°C–800°C, indicating that the amorphous structure has not changed over this temperature range. This phenomenon shows that the strength decrease of GP in the process of rising calcination temperature is mainly related to water evaporation. For BSRGP1 in Fig. 8b, from room temperature to 600°C, there is almost no difference in the XRD patterns of the samples, but at 800°C, there is a small amount of characteristic diffraction peaks of nepheline, indicating that a small amount of sintering occurs after calcination at this temperature, and BS is oxidized in the interior without significant influence on the material structure.

In addition, there is almost no difference between Figs. 8a and 8b from room temperature to 600°C. This indicates that the phase composition of both GP and BSRGP1 are almost unchanged in this temperature range, the compressive strength of BSRGP1 is slightly higher than that of GP may be due to the voids caused by water evaporation are filled by BS-burning carbides. As shown in Fig. 4a, although the compressive strength gradually decreases with the increase of temperature, the compressive strength of BSRGP1 is obviously higher than that of GP at 800°C, which is related to the small amount of nepheline crystals produced at this temperature.

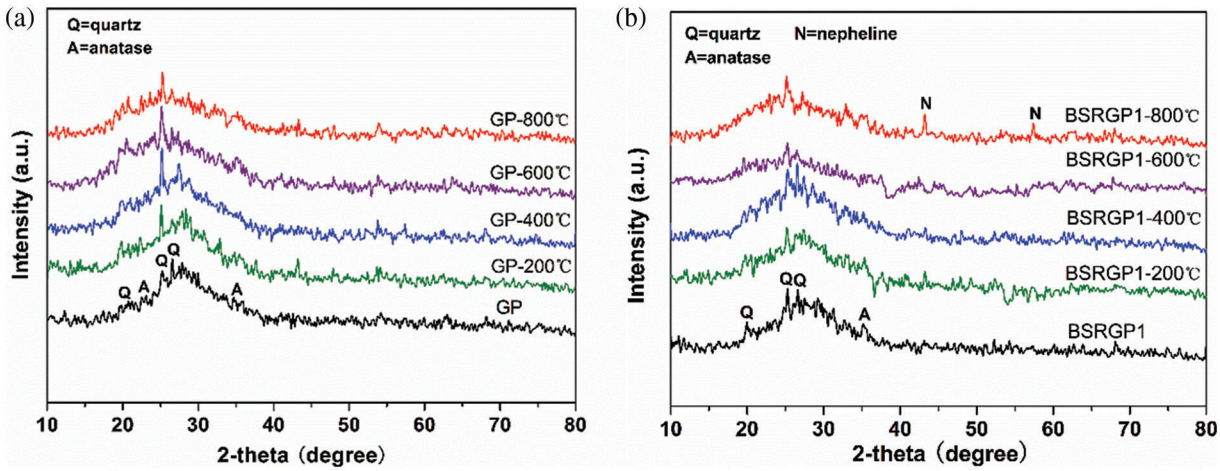

Figure 8: XRD patterns for GP and BSRGP1 at different temperatures

4 Conclusions

In this work, the effects of bamboo shaving on the physical performance, micro-structure, and mechanical strengths of geopolymer composites at different temperatures (including room temperature and 200°C–800°C) were studied. The conclusions from the experiment study are as follows:

(1) According to TGA analysis results, bamboo shaving does not significantly affect the thermos-stability of the metakaolin based geopolymer, the residual weigh of bamboo shaving geopolymer composites at 800°C is only 3% lower than that of pure geopolymer.

(2) With the temperature increasing, the dry shrinkage, porosity, and water absorption of the geopolymer composites increase, while the density decrease, which is related to the light weight and water absorption of bamboo shaving. Compressive and flexural strengths of pure geopolymer and bamboo shaving reinforced geopolymer composites all decrease after exposure to the elevated temperature, and the flexural strength decrease more significantly.

(3) The physical degradation of bamboo shaving and shrinkage of geopolymer matrix induced by high-temperatures exposure are the determinal factors that control the loss of mechanical strength.

The preliminary study in this study shows that bamboo shaving has great development potential as reinforcer for low-cost geopolymer matrix composites, and it is recommended to be used for application up to 400°C. Nevertheless, further research is needed on the mechanical properties at elevated temperature to verify this.

Funding Statement: This work was supported by the Excellent Youth Foundation of Education Department of Hunan Province, China (20B612) and Changsha Natural Science Foundation of China (kq2014158).

Conflicts of Interest: The authors declare that they have no conflicts of interest to report regarding the present study.

References

1. Kodur, V. (2014). Properties of concrete at elevated temperatures. *ISRN Civil Engineering, 2014(2),* 1–15. DOI 10.1155/2014/468510.
2. Shaikh, F. U. A., Vimonsatit, V. (2015). Compressive strength of fly-ash-based geopolymer concrete at elevated temperatures. *Fire & Materials, 39(2),* 174–188. DOI 10.1002/fam.2240.

3. Martin, A., Pastor, J. Y., Palomo, A., Fernández Jiménez, A. (2015). Mechanical behavior at high temperature of alkali-activated aluminosilicates (geopolymer). *Construction and Building Materials, 93,* 1188–1196. DOI 10.1016/j.conbuildmat.2015.04.044.
4. Davidovits, J. (1991). Geopolymers: Inorganic polymeric new material. *Journal of Thermal Analysis and Calorimetry, 37(8),* 1633–1656. DOI 10.1007/BF01912193.
5. Shaikh, F. U. A. (2013). Review of mechanical properties of short fibre reinforced geopolymer composites. *Construction and Building Materials, 43,* 37–49. DOI 10.1016/j.conbuildmat.2013.01.026.
6. Frydrych, M., Hýsek, S., Fridrichová, L., van, S. L., Herclík, M. et al. (2020). Impact of flax and basalt fibre reinforcement on selected properties of geopolymer composites. *Sustainability, 12(1),* 118. DOI 10.3390/su12010118.
7. Chu, S. H., Ye, H., Huang, L., Li, L. G. (2021). Carbon fiber reinforced geopolymer (FRG) mix design based on liquid film thickness. *Construction and Building Materials, 269,* 121278. DOI 10.1016/j.conbuildmat.2020.121278.
8. Li, L. G., Xiao, B. F., Fang, Z. Q., Xiong, Z., Chu, S. H. et al. (2021). Feasibility of glass/basalt fiber reinforced seawater coral sand mortar for 3D printing. *Additive Manufacturing, 37,* 101684. DOI 10.1016/j.addma.2020.101684.
9. Rashad, A. M. (2019). The effect of polypropylene, polyvinyl-alcohol, carbon and glass fibres on geopolymers properties. *Materials Science and Technology, 35(2),* 127–146. DOI 10.1080/02670836.2018.1514096.
10. Silva, G., Kim, S., Aguilar, R., Nakanatsu, J. (2019). Natural fibers as reinforcement additives for geopolymers–A review of potential eco-friendly applications to the construction industry. *Sustainable Materials and Technologies, 23,* e00132. DOI 10.1016/j.susmat.2019.e00132.
11. Korniejenko, K., Mucsi, G., Halyag, N. P., Szabó, R., Mierzwiński, D. et al. (2020). Mechanical properties of basalt fiber reinforced fly ash-based geopolymer composites. *RICON19-REMINE International Conference on Valorization of Mining and Industrial Wastes into Construction Materials by Alkali-Activation*, pp. 86–100. Covilhã, Portugal. KnE Engineering. DOI 10.18502/keg.v5i4.6800.
12. Sun, P. J., Wu, H. C. (2008). Transition from brittle to ductile behavior of fly ash using PVA fibers. *Cement & Concrete Composites, 30(1),* 29–36. DOI 10.1016/j.cemconcomp.2007.05.008.
13. Moradikhou, A. B., Esparham, A., Avanaki, M. J. (2020). Physical & mechanical properties of fiber reinforced metakaolin-based geopolymer concrete. *Construction and Building Materials, 251,* 118965. DOI 10.1016/j.conbuildmat.2020.118965.
14. Alomayri, T., Low, I. M. (2013). Synthesis and characterization of mechanical properties in cotton fiber-reinforced geopolymer composites. *Journal of Asian Ceramic Societies, 1(1),* 30–34. DOI 10.1016/j.jascer.2013.01.002.
15. Łach, M., Hebdowska-Krupa, M., Mierzwiński, D., Korniejenko, K. (2019). Mechanical properties of geopolymers reinforced with carbon and aramid long fibers. *IOP Conference Series: Materials Science and Engineering, 706,* 012011. DOI 10.1088/1757-899X/706/1/012011.
16. Zhao, J., Wang, K., Wang, S. B., Wang, Z. K., Yang, Z. H. et al. (2021). Effect of elevated temperature on mechanical properties of high-volume fly ssh-based geopolymer concrete, mortar and paste cured at room temperature. *Polymers, 13,* 1473. DOI 10.3390/polym13091473.
17. Sankar, K., Kriven, W. M. (2017). Geopolymer reinforced with E-glass leno weaves. *Journal of the American Ceramic Society, 100(6),* 1–10. DOI 10.1111/jace.14783.
18. Welter, M., Schmucher, M., MacKenzie, K. J. D. (2015). Evolution of the fibre-matrix interactions in basalt-fibre-reinforced geopolymer-matrix composites after heating. *Journal of Ceramic Science and Technology, 6(1),* 17–24. DOI 10.4416/JCST2014-00034.
19. Behera, P., Baheti, V., Militky, J., Louda, P. (2018). Elevated temperature properties of basalt microfibril filled geopolymer composites. *Construction and Building Materials, 163,* 850–860. DOI 10.1016/j.conbuildmat.2017.12.152.
20. Behera, P., Baheti, V., Militky, J., Naeem, S. (2018). Microstructure and mechanical properties of carbon microfiber reinforced geopolymer at elevated temperatures. *Construction and Building Materials, 160,* 733–743. DOI 10.1016/j.conbuildmat.2017.11.109.
21. Tanyildizi, H., Yonar, Y. (2016). Mechanical properties of geopolymer concrete containing polyvinyl alcohol fiber exposed to high temperature. *Construction and Building Materials, 126,* 381–387. DOI 10.1016/j.conbuildmat.2016.09.001.

22. Celik, A., Yilmaz, K., Canpolat, O., AI-mashhadani, M. M., Aygörmez, Y. et al. (2018). High-temperature behavior and mechanical characteristic of boron waste additive metakaolin based geopolymer composites reinforced with synthetic fibers. *Construction and Building Materials, 187,* 1190–1203. DOI 10.1016/j.conbuildmat.2018.08.062.
23. Alomayri, T., Vickers, L., Shaikh, F. U. A., Low, I. M. (2014). Mechanical properties of cotton fabric reinforced geopolymer composites at 200°C–1000°C. *Journal of Advanced Ceramics, 3(3),* 184–193. DOI 10.1007/s40145-014-0109-x.
24. He, P. G., Jia, D. C., Lin, T. S., Wang, M. R., Zhou, Y. (2010). Effects of high-temperature heat treatment on the mechanical properties of unidirectional carbon fiber reinforced geopolymer composites. *Ceramics International, 36(4),* 1447–1453. DOI 10.1016/j.ceramint.2010.02.012.
25. Rickard, W. D. A., Vickers, L., Riessen, A. V. (2013). Performance of fibre reinforced, low density metakaolin geopolymers under simulated fire conditions. *Applied Clay Science, 73,* 71–77. DOI 10.1016/j.clay.2012.10.006.
26. Kong, D. L. Y., Sanjayan, J. G., Sagoe-Crentsil, K. (2007). Comparative performance of geopolymers made with metakaolin and fly ash after exposure to elevated temperatures. *Cement and Concrete Research, 37(12),* 1583–1589. DOI 10.1016/j.cemconres.2007.08.021.
27. Bakharev, T. (2005). Geopolymeric materials prepared using class F fly ash and elevated temperature curing. *Cement Concrete Research, 35(6),* 1224–1232. DOI 10.1016/j.cemconres.2004.06.031.
28. Zhang, J. Y., Li, Z. Y., Zhang, X. L. (2022). Synthesis and characterization of a novel bamboo shaving geopolymer composite. *Journal of Renewable Materials, 10(11),* 2871–2881. DOI 10.32604/jrm.2022.019373.
29. Haykiri-Acma, H., Yaman, S. (2007). Synergy in devolatilization characteristics of lignite and hazelnut shell during co-pyrolysis. *Fuel, 86(3),* 373–380. DOI 10.1016/j.fuel.2006.07.005.
30. Yang, H. P., Yan, R., Chen, H. P., Lee, D. H., Zheng, C. G. (2007). Characteristics of hemicellulose, cellulose and lignin pyrolysis. *Fuel, 86(12–13),* 1781–1788. DOI 10.1016/j.fuel.2006.12.013.
31. Short, N. R., Purkiss, J. A., Guise, S. E. (2001). Assessment of fire damaged concrete using colour image analysis. *Construction and Building Materials, 15,* 9–15. DOI 10.1016/S0950-0618(00)00065-9.
32. Alomayri, T., Shaikh, F. U. A., Low, I. M. (2013). Characterisation of cotton fibre-reinforced geopolymer composites. *Composites: Part B, 50,* 1–6. DOI 10.1016/j.compositesb.2013.01.013.
33. Silva, G., Kim, S., Castañeda, A., Donayre, R., Nakamatsu, J. et al. (2018). A comparative study of linen (Flax) fibers as reinforcement of Fly Ash and clay brick powder based geopolymers. *IOP Conference Series: Materials Science and Engineering, 416,* 012107. DOI 10.1088/1757-899X/416/1/012107.
34. Roviello, G., Ricciotti, L., Ferone, C., Colangelo, F., Tarallo, O. (2015). Fire resistant melamine based organic-geopolymer hybrid composites. *Cement & Concrete Composites, 59,* 89–99. DOI 10.1016/j.cemconcomp.2015.03.007.